American Mineralogist, Volume 95, pages 1006–1016, 2010

The computation of equilibrium assemblage diagrams with Theriak/Domino software

Christian de Capitani[1,*] and Konstantin Petrakakis[2]

[1]Mineralogisch-Petrographisches Institut, Universität Basel, Bernoullistrasse 30, CH-4056 Basel, Switzerland
[2]Department of Geological Sciences, University of Vienna, Althanstrasse 14, A-1090 Vienna, Austria

Abstract

In this paper, the term "equilibrium assemblage diagrams" refers to diagrams strictly based on assemblages predicted by Gibbs free energy minimization. The presented Theriak/Domino software uses a unique algorithm of scanning and bookkeeping, which allows to compute completely and automatically a great variety of diagrams: phase diagrams, pseudo-binary, pseudo-ternary, isopleths, modal amounts, molar properties of single phases or bulk-rock properties like total ΔG, volume of solids, etc. The speed and easiness of use makes thermodynamic modeling accessible to any student of Earth sciences and offers a powerful tool to check the consistency of thermodynamic databases, develop new solution models, plan experimental work, and to understand natural systems. The examples described in this paper demonstrate the capacity of the software, but also to show the usefulness and limitations of computed equilibrium assemblage diagrams. For most illustrations, a metapelite (TN205) from the eastern Lepontine Alps is used. The applications include the interpretation of complex diagrams, mineral reactions, the effect of Al content on the equilibrium assemblages, the interpretation of Si per formula unit in white mica, understanding some features of garnet growth, dehydration and isothermal compressibility, a broadening of the concept of AFM diagrams, combining equilibrium assemblage diagram information with thermobarometry, and comparing the results produced with different databases. Equilibrium assemblage diagrams do not always provide straightforward answers, but mostly stimulate further thought.

Keywords: Phase diagram, software, Gibbs free energy minimization, equilibrium assemblage, metapelites

Introduction

For over a hundred years, it has been recognized that mineral assemblages depend on temperature, pressure, and bulk composition of the rocks (e.g., Becke 1904; Goldschmidt 1912a, 1912b; Eskola 1915, 1922; Grubenmann and Niggli 1924). Different concepts, such as depth zones or mineral facies, were introduced to classify and understand metamorphic evolution and to relate equilibrium mineral assemblages to bulk-rock compositions and conditions of rock formation. These concepts were purely descriptive and although based upon the theory of chemical equilibrium, a thermodynamic analysis remained for a long time unachievable. Today, after decades of experimental work providing thermodynamic data and the availability of powerful computers, we are capable of predicting complex assemblages and compute diagrams that visualize these relations. Among the numerous computer programs used by petrologists, four are particularly popular: THERMOCALC (Powell et al. 1998; Powell and Holland 1994), Perple_X (Connolly 1990), Theriak/Domino (de Capitani and Brown 1987; de Capitani 1994) and Gibbs (Spear et al. 2001). Some others, not mentioned here, either focus more on aqueous geochemistry or metallurgy, or are for commercial use.

The aim of this paper is to present the Theriak/Domino software with focus on Domino and its algorithm. The capabilities of the software will be presented by means of sample applications. Although the software has been available for some time, it has only recently reached some state of robustness and user-friendliness that makes it accessible not only to a few specialized theoreticians, but also practically to every Earth scientist. The benefit of Domino is that not only the calculation, but also the graphical representation of the results, are done automatically with practically no user intervention.

Domino is part of the Theriak/Domino software package that consists of 10 programs. The core of the program package is Theriak, which calculates equilibrium assemblages for a given bulk-rock composition at any P and T. The strategy of Theriak is linear programming combined with minimization of single thermodynamic solution functions and is designed to produce the correct assemblage even for extremely complex, non-ideal systems. Its algorithm has been described earlier by de Capitani and Brown (1987). The emphasis of this paper is, however, on the program Domino, which computes equilibrium assemblage diagrams. The term "equilibrium assemblage diagrams" is used here exclusively for diagrams based on Gibbs free energy minimization.

Equilibrium assemblage diagrams

In an equilibrium assemblage diagram, each point defines a unique bulk composition, P and T. The diagram maps the predicted stable assemblages based on Gibbs free energy minimization. Contrary to classical petrogenetic grids, a corresponding equilibrium assemblage diagram is valid only for a particular bulk-rock composition. In turn, because each field defines

* E-mail: christian.decapitani@unibas.ch

exactly one assemblage, they are a lot easier to understand than petrogenetic grids. The stability fields calculated by Domino are based on Gibbs free energy minimization rather, than on solving complex systems of equations. This technique reflects the fundamental principle of thermodynamics that relates stability of an assemblage with minimal energy content. In summary, an equilibrium assemblage diagram is a prediction (based on thermodynamic properties given in a database) of which assemblages are stable for a specific rock under specific conditions. Because current databases are still a far way from being perfect and covering all possible phase compositions, these predictions are fairly simplified models, rather than accurate reproductions of natural systems. Nevertheless, equilibrium assemblage diagrams are powerful tools to: (1) check and visualize the implications of thermodynamic databases; (2) develop new equations of state and solution models; (3) plan experimental work; and (4) understand natural systems.

THE THERIAK/DOMINO SOFTWARE PACKAGE

The Theriak/Domino package includes several programs for thermodynamic calculations and plotting of results in graphical form. The most important are Theriak and Domino. Theriak calculates the equilibrium mineral assemblage and phase compositions for a given rock-bulk composition at specified *P*-*T* or along a *P*-*T* path. Domino calculates equilibrium assemblage diagrams for selectable axes (*P*, *T*, component activities, or compositions) as well as pseudo-binary or pseudo-ternary phase diagrams, pixelmaps of thermodynamic variables and isolines for bulk-rock, mineral, and solution properties. The expressions pseudo-binary and pseudo-ternary are used for diagrams that show a variation between two or three bulk chemical compositions. Strictly speaking, the prefix "pseudo" is only justified if some of the calculated stable phases are not linear combinations of these bulk chemical compositions.

The latest version (010809) of the software offers on-line help as well as a reworked manual. The Theriak/Domino package, including source code and examples, is available for free download for non-commercial purposes from http://titan.minpet.unibas.ch/minpet/theriak/theruser.html.

Strategy of Domino

The basic strategy is a systematic scan of the diagram, in which equilibrium assemblages are computed by calling the program Theriak. Recognition and smoothing of reaction curves and preparation of results for a graphical plot is based on the unique bookkeeping of Domino. For a better understanding of the algorithm, some expressions used by the program and written into its output files should be explained.

Assemblage. The definition of an assemblage is very flexible. For example, assemblage1 might be defined as "staurolite present" and assemblage2 as "staurolite absent." Such a definition would outline the staurolite stability field for a given bulk composition. For isolines calculations for example, the term "assemblage" refers to a specific range of compositions or modal amounts of a certain phase. Each time a new assemblage is found, it is added to an assemblage list and further referred to by its number.

Reaction. Each time Domino finds a transition between two assemblages a "reaction" is defined. The meaning of a "reaction" is of course strongly dependent on the assemblage definition.

Point. The coordinates where a reaction occurs define a "point." The spatial resolution is usually 0.005 cm. Besides the x- and y-values, the point is also assigned the corresponding reaction number, the level of refinement and the labels of the two neighboring grid rectangles (see below for details).

Line. A line is a succession of points, which in connection produce a line in the diagram. A single reaction may be split into several "lines." Finding the order in which the points calculated are to be connected to produce lines is an essential task of the Domino algorithm illustrated in Figure 1.

First approximation of diagram construction

Consider a diagram with three assemblages separated by three reactions (Fig. 1a). First the xy-space is divided into rectangles by a regular grid. For the sake of simplicity, the grid in Figure 1a is a 5 × 5 grid. The rectangles are numbered and labeled according to their row and column position. For example, rectangle (3/2) is the third in x- and second in y-direction. The diagram is then scanned along the grid and equilibrium assemblages are calculated at each grid point (Fig. 1b). A change of the assemblage from one grid point to the next indicates that at least one reaction point occurs in between. Refinement of the position of these points is accomplished by interval halving until the required spatial resolution is obtained. To construct a diagram, several bookkeeping parameters must be assigned to each point (Fig. 1c). For instance, the first point found (point 1) belongs to reaction 1, separating assemblages 1 and 2, and the adjacent rectangles at level zero of refinement are (2/0) and (2/1). Point 10 belongs to the same reaction and is at the boundary of rectangles (2/1) and (3/1). This information is allocated to each point and then used to identify individual lines. Figure 1d shows how lines are constructed by connecting points of the same reaction that share a common neighboring rectangle (this strategy is reminiscent of the game of dominoes, hence the name of the program). In the present example, three lines are found: line 1 (pts 1-10-2-3), line 2 (pts 11-4-9-8), and line 3 (pts 5-12-6-13-7).

Refinement of diagram

Figure 1e is a first graphical approximation of the equilibrium assemblage diagram. The next task Domino performs is to examine all lines that require refinement. Smoothness is tested using the angle defined by three consecutive points p1, p2, and p3. If the angle $\angle$(p1,p2,p3) is smaller than a minimum, this is recognized as a "bump" and the rectangles adjoining are identified for further refinement. The test revealing a bump is: $\cos(\gamma) > (4w^2 - c^2)/(4w^2 + c^2)$, where γ is the angle at p2, c is the distance between p1 and p3, and w is the "angular precision," by default 0.04 cm. "Open ends" are points at the end of a line but not on the border of the diagram. The unshared rectangle is also set apart for refinement. In addition, if a line is only defined by two points, the square between them will also need closer examination.

The grid-length is now halved and the diagram is divided into smaller rectangles. In Figure 1f, the rectangles identified for refinement are shaded; these will be used to calculate new reaction points. However, before we can proceed, all previously calculated points must be assigned the new rectangles from the smaller grid (Fig. 1g). Point 1 is assigned (3/0) and (3/1), point

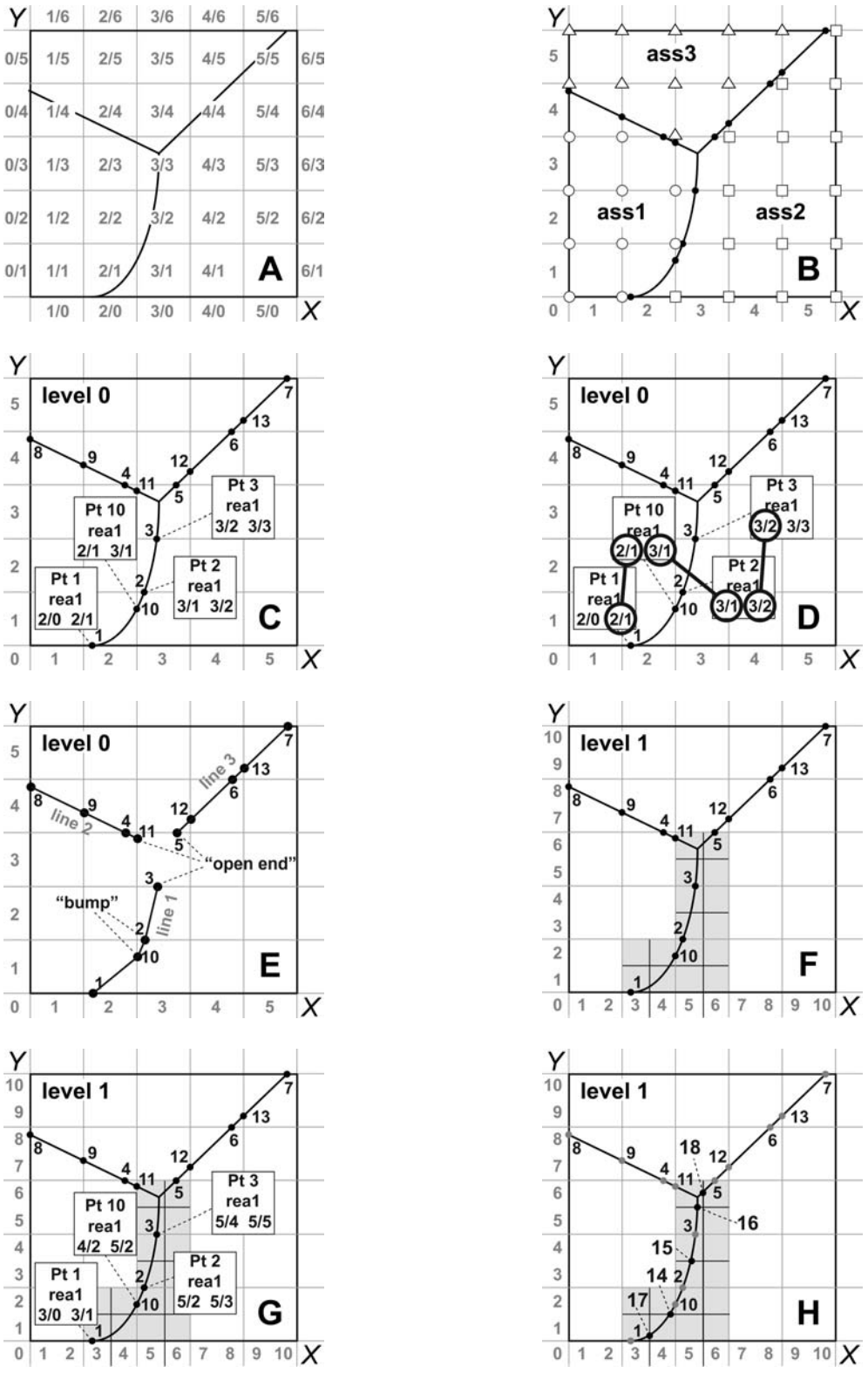

FIGURE 1. Sketch of the Domino algorithm. See text for details. (**a**) Sample diagram with definition of initial grid. (**b**) Assemblages and points found along the initial grid. (**c**) Assigning reactions and rectangles to each point. (**d**) Connecting points sharing one neighboring rectangle. (**e**) Identifying which rectangles need refinement. (**f**) Defining a new grid with smaller rectangles. (**g**) Assigning new rectangles to all points. (**h**) Adding points found along the smaller grid.

10 is assigned (4/2) and (5/2), etc. Next, each of the identified rectangles is scanned across the middle horizontally and vertically for new points (Fig. 1h). Again, each point is assigned a reaction number, a refinement level and the two adjoining rectangles. The lines are rebuilt, using all points searching for common neighboring squares as already described for Figure 1d. The process of refinement is repeated (typically five times) until, within the desired spatial resolution, the polygonal bumps are smoothened and open ends are removed.

Comments to the Domino strategy

The flexible definition of "assemblage" allows one to calculate very different types of diagrams: phase diagrams, pseudo-binary, pseudo-ternary, isopleths, modal amounts, molar properties of single phases or bulk-rock properties like total ΔG, volume of solids, etc. The only restriction for the x- and y-axes are that for each point in the diagram P, T, and the bulk composition must be uniquely defined. Possible variables are P, T, component activities, and bulk compositional variations.

If one reaction enters and leaves a rectangle between two grid points of the initial grid, this is not recognized in the first scan and the segment inside the rectangle will be missing in the final diagram. This happens occasionally, but can be repaired by either reducing the length of the initial grid or by recalculating the missing segment separately.

If two reactions' curves are almost parallel and extremely close to each other, i.e., within the spatial resolution of the program (<0.005 cm), Domino will randomly either distinguish and handle them separately or combine them and treat them as one reaction. The result is an intermittent line alternating between one and two reactions. This increases computation time, but the diagrams are still perfectly readable.

Examples of equilibrium assemblage diagrams

For comparison of computing times, all examples were calculated on a MacBook Pro 2.4 GHz Intel Core 2 Duo with an Intel Compiler. Labeling of the stability fields was done manually with a graphics editor.

Sample TN205

Sample TN205 from Nagel et al. (2002) will be repeatedly used in the following to demonstrate the capabilities of Theriak/Domino. This metapelite was collected from the second staurolite zone in the eastern Lepontine Alps and is rich in K and Na, with a low K/(K+Na) ratio of 0.51 and a high Fe/(Fe+Mg) ratio of 0.72. It contains garnet, white mica, biotite, staurolite, paragonite, plagioclase, quartz, chlorite and accessory ilmenite, rutile, and apatite. The matrix assemblage is Grt-Ms-Bi-Qtz-Pl-St. Relics of a high-pressure assemblage are Grt-Ms-Pg. Contrary to other metapelites from the same area, this sample does not contain kyanite. Staurolite is observed to grow at the expense of paragonite. The *P-T* evolution of this rock is described in Nagel et al. (2002) and is similar to TN291, for which some diagrams were published. The database used here is JUN92 (based on Berman 1988) with improved solution models for white mica (Keller et al. 2005) and chlorite (Hunziker 2003). The (simplified) bulk composition in moles of TN205 is Si(50.36), Al(30.54), Fe(6.23), Mg(2.46), Ca(1.07), Na(4.62), K(4.73), and O(160.965). For the calculations, excess water was added.

As stated earlier, equilibrium assemblage diagrams always relate to a specific bulk composition. They illustrate which assemblages would theoretically be stable at equilibrium. Obviously, these diagrams do not exactly describe what happens in nature; they merely serve as models that help understand natural processes. Fortunately, many metamorphic rocks show a dominant assemblage, which we believe to have formed around peak metamorphic conditions. If the rock has reached equilibrium and post-peak processes have not modified the mineral compositions, calculation of an equilibrium assemblage diagram with Theriak/Domino helps to constrain the *P-T* conditions for this assemblage. Further information that we may deduce from a diagram include precursor minerals, *P-T* ranges for relics, and constraints on the post-peak path. To understand the information provided by complex equilibrium assemblage diagrams, such as the one shown in Figure 2a, one has to spend some time on its interpretation. The program Theriak will provide detailed information about amounts and compositions of phases forming an equilibrium assemblage just by entering any pressure and temperature. Contrary to petrogenetic grids or thermobarometry results, the first focus here is not on single reactions, but on the equilibrium assemblages. In Figure 2a, the larger fields are labeled with the stable phases. The first assemblages to look for are those observed in the sample thin sections. In case of TN205, the matrix assemblage Grt-Ms-Bi-Qtz-Pl-St is found in Figure 2a around 600 °C and 7 kbar. Furthermore, the relic high-pressure assemblage Grt-Ms-Pg-Qtz occupies a large stability field above 14 kbar. These findings suggest an overall decompression at ca. 600 °C from 14 to 7 kbar. To some extent, equilibrium assemblage diagrams provide us with suggestions of minerals and reactions we might look for in our samples. For instance, decompression from the high-pressure assemblage might first grow plagioclase, then staurolite and finally biotite, or, along a different path, first grow biotite, then plagioclase followed by staurolite. Both paths end with the same matrix assemblage (Grt-Ms-Bi-Qtz-Pl-St). An obvious feature in Figure 2a is the amazingly large stability field of garnet coexisting only with phases typically not containing Fe and Mg. This is a common observation not only for the specific rock composition TN205, but also for metapelites in general and will be discussed shortly along with the capability of Domino to calculate pseudo-AFM diagrams.

To understand mineral reactions better, it might be practical to outline the stability fields of single minerals with a graphics editor. Figure 2b shows the stability fields of white mica and feldspar. The Pg-Ab and Ms-Kfs dehydration reactions that take place with increasing temperature can be easily recognized. The paragonite stability field shows more or less the same extent as in many other calculations for different metapelites. This is because Pg-rich white mica shows only very little chemical variability (90–100% Pg). A similar observation can be made for the transition of K-rich white mica to K-feldspar. On the other hand, the plagioclase field, and therefore its overlap with Pg, depends strongly on bulk composition.

In Figure 2c, the stability fields of the Al-rich phases kyanite, sillimanite, staurolite, and cordierite are outlined. With increasing temperature or decompression, these phases grow as paragonite breaks down. The predicted overlap of paragonite with staurolite

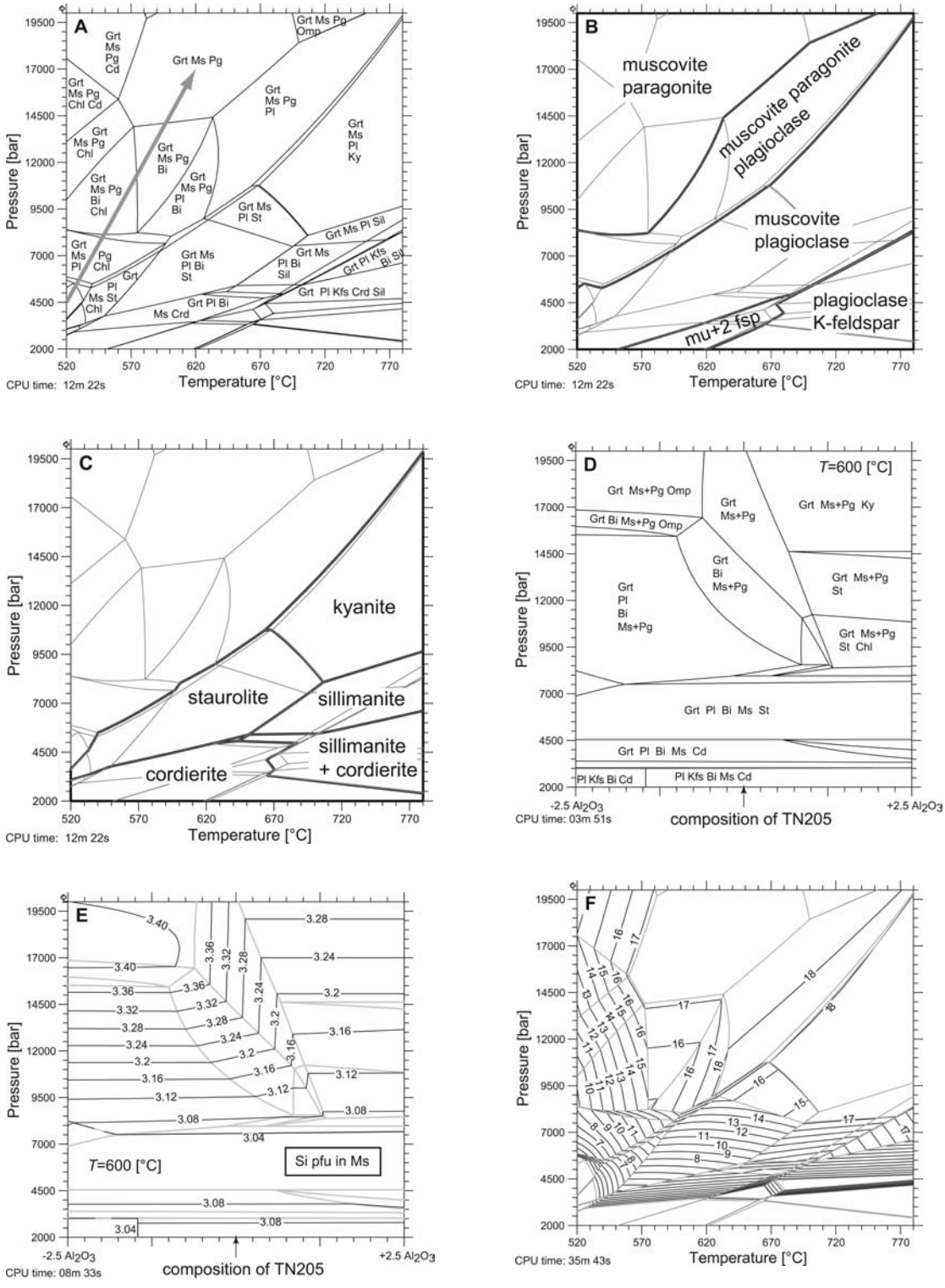

FIGURE 2. Examples of equilibrium assemblage diagrams computed by Domino for sample TN205. All assemblages coexist with excess H_2O and Qtz. Bi = biotite, Chl = chlorite, Grt = garnet, Kfs = K-feldspar, Ky = kyanite, Ms = muscovite, Pg = paragonite, Pl = plagioclase, Sil = sillimanite, St = staurolite, Omp = omphacite. (**a**) Equilibrium assemblage diagram, the arrow indicates the path used in Figure 4. (**b**) Outlines of stability fields for white mica and feldspar; (**c**) stability fields of kyanite, sillimanite, staurolite and cordierite. (**d**) Pseudo-binary diagram calculated at T = 600 °C showing the effect of bulk Al variation on the equilibrium of assemblages related to the input bulk composition TN205 (cf. **a**). (**e**) Pseudo-binary at T = 600 °C with isolines of Si per formula unit of Ms, (**f**) isolines of vol% of garnet (modal amount).

and kyanite is very small, and staurolite and sillimanite show no overlap at all. This is not quite consistent with the frequently observed occurrence of staurolite and kyanite. [Nagel et al. (2002) suggest metastable kyanite growth from paragonite breakdown inside the staurolite field.]

To investigate the effect of system component variations on the stable assemblages, it is possible to calculate pseudo-binary diagrams with Domino. Figure 2d for example, shows such dependence for the Al content in metapelites. The two pseudo-binary end-member compositions are defined simply by increasing and decreasing the Al content of TN205 by 2.5 moles, which results in compositions typical for high-Al and low-Al metapelites. Figure 2d makes the distinction between these two rock types immediately evident. Low-Al metapelites (left side) show biotite stable at high pressures, high-Al metapelites (right side) have staurolite stable. Superimposed on the pseudo-binary in Figure 2e are isolines of Si per formula unit of muscovite (K-rich white mica). This number is sometimes used as a minimum pressure indicator. A more accurate pressure estimation is only possible for rocks containing the assemblage, which was used to calibrate this geobarometer, i.e., phengite + biotite + feldspar + quartz (Massonne and Schreyer 1987; Coggon and Holland 2002). The dependence on pressure is clearly visible, but also the fact that the Si content of white mica is strongly dependent on bulk chemistry and mineral assemblage. For example, contrary to any uncritical expectation, the Si apfu of white mica for the high-pressure assemblage Grt-Ms-Pg-Qtz-H_2O in TN205 is solely dependent on bulk composition, but not on pressure.

For discussions on mineral growth, a useful feature of Domino is the calculation of isopleths or modal isolines. As an example, the modal amount of garnet expressed as vol% of solids is shown in Figure 2f. An interesting observation is that above 12 kbar and 570 °C, the amount of garnet remains almost constant. Another implication we may infer from Figure 2f is that, for the period of decompression, garnet growth is very limited but not impossible. Diagrams of the type shown in Figures 2d–2f have been presented by numerous authors, using many different methods of calculation [Spear and Markussen (1997), Meyre et al. (1997), Spear et al. (1999), Tinkham et al. (2001), Coggon and Holland (2002), Spear (2004), and Pattison and Tinkham (2009)].

Because of the brute force method used, isolines may take several hours to compute. A quicker overview on variation of all variables can be gained with the creation of so-called pixelmaps. This uses a very simple algorithm built into Domino that scans the diagram over a regular grid (e.g., 100 × 100) and stores all the information on the assemblages found in separate files. An auxiliary program generates gray pixelmaps for any desired variable. Figure 3 shows two examples of pixelmaps. Figure 3a is the wt% of water in the solids, which visualizes the main dehydration reactions already seen in Figure 2b. The second example is the isothermal compressibility coefficient [$-1/V\,(\mathrm{d}V/\mathrm{d}P)$] calculated through the volume difference of two adjacent points. Both gray pixelmaps contain information that may be very useful for the discussion of rock evolution, for example in subduction zones. Dehydration and density information might correlate with earthquake locations and observed seismic velocities. This type of Domino calculation has been used by Bousquet et al. (2005).

To have a closer look at prograde or retrograde variations of mineral properties, we can calculate equilibrium assemblages along a pre-defined *P*-*T* path and plot selected variables. Figure 4 shows mineral modes and garnet compositions in 100 steps along a path from 520 °C/4.5 kbar to 620 °C/17 kbar for sample TN205. For each step in Figure 4a complete equilibrium is assumed. In Figure 4b the same path is used, however, after each step any newly grown garnet is removed from the bulk composition. This fractionation model helps in understanding garnet zonations and the consequences of changes in effective bulk composition along a prograde path. The first major garnet growth spurt is predicted to occur around 5.5 kbar at the breakdown of chloritoid. This is followed by continuous growth at the expense of chlorite and feldspar and leads to a second major growth at around 8–8.5 kbar, when feldspar becomes unstable. At that point, the garnet composition shows a noticeable increase of the grossular component, a feature sometimes observed in zoned garnets. Because there is no Mn, or other strongly fractionating element in the system, the

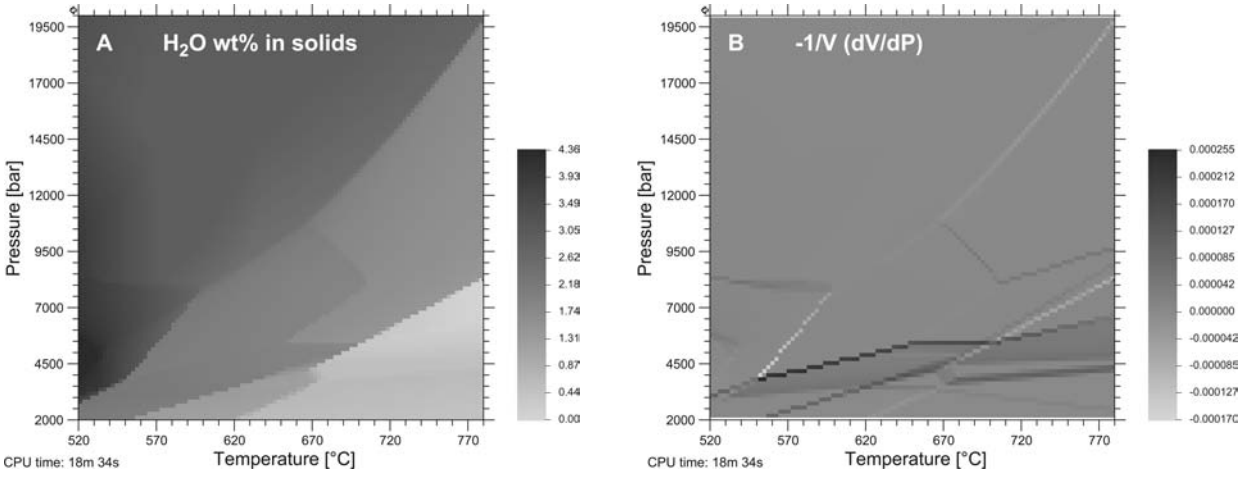

FIGURE 3. Examples of pixelmaps computed by Domino using the composition of sample TN205. (**a**) Gray pixelmap of water content of solids (wt%); (**b**) gray pixelmap of isothermal compressibility coefficient.

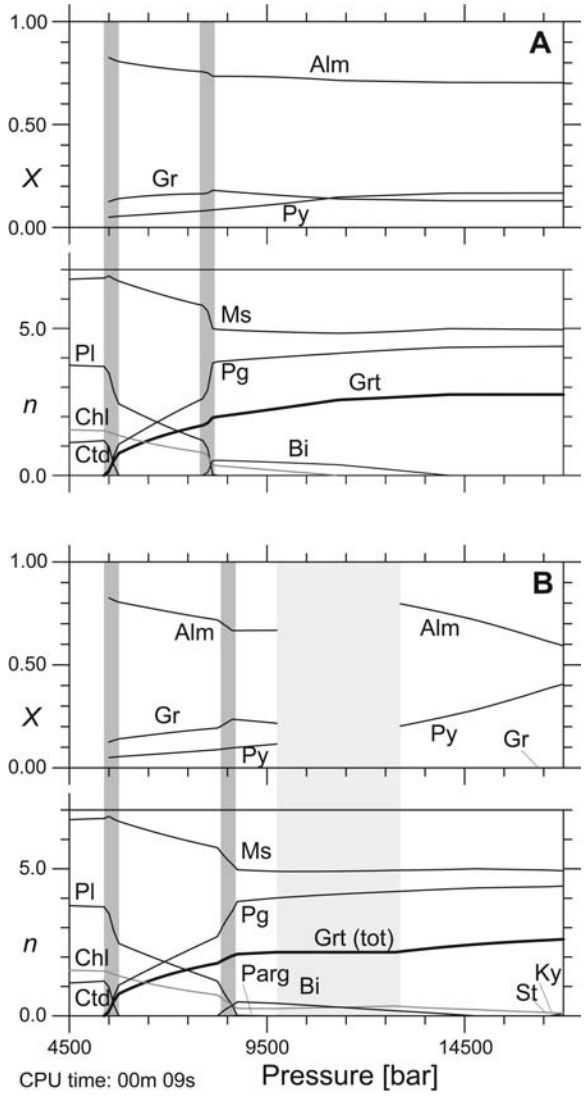

Figure 4. Equilibria calculated along the *P-T* path indicated in Figure 2a: (**a**) assuming complete equilibrium at each step, (**b**) fractionation of garnet; at each step the composition of the newly grown garnet is subtracted from the bulk composition. Alm = almandine, Bi = biotite, Chl = chlorite, Ctd = chloritoid, Gr = grossular, Grt = garnet, Ky = kyanite, Ms = muscovite, Parg = pargasite, Pg = paragonite, Pl = plagioclse, Py = pyrope, St = staurolite. n is the modal amount of the phases, x is the composition of growing garnet. The light-shaded area is a *P-T* segment where garnet is not growing and x is not defined.

equilibrium and the fractionation model are surprisingly similar. Between 10 and 13 kbar, complete fractionation shows no further growth and, because all Ca of the system is bound to the garnet core, the last rim is completely Ca-free. In addition, the fractionation yields very small amounts of paragonite around 9 kbar and kyanite and staurolite above 16.5 kbar. A more realistic approach, also based on the Theriak/Domino software, considering diffusion and re-equilibration to numerically model prograde garnet growth was presented by Gaidies et al. (2008a, 2008b).

Pseudo-AFM diagrams

A popular way to investigate phase relations in metapelites is the use of AFM diagrams (Thompson 1957). To demonstrate the capability of Domino to explore compositional space with pseudo-ternary diagrams we present two equilibrium assemblage diagrams, which are deceptively similar to AFM.

With SiO_2 and H_2O in excess, we consider the compositional tetrahedron K_2O-Al_2O_3-FeO-MgO. A true AFM diagram is a projection of all stable assemblages from muscovite (or, at high temperatures from K-feldspar) to the AFM projection plane. Geometrically, the tie-lines from muscovite are extended and cut with the Al_2O_3-FeO-MgO ternary. Defining a pseudo-ternary section through the tetrahedron, which cuts the same tie-lines will produce an equilibrium assemblage diagram that is topologically identical. To construct such a pseudo-AFM diagram, muscovite cannot be an end-member of a solution phase and therefore the commonly used white mica solution model is temporarily removed from the database. Furthermore, the section must be chosen through assemblages that all contain muscovite. This choice is not unique. For Figure 5a, the lower left corner ("F") is defined as K-feldspar+FeO, the lower right corner ("M") is K-feldspar+MgO, and ("A") is Al_2O_3. All corners contain additional excess SiO_2 and H_2O. The result at 600 °C and 18 kbar (Fig. 5a) is equivalent to a classical AFM diagram, because all assemblages contain muscovite, quartz, and water. To push the calculations to the next level, we abandon the concept of the AFM projection completely, and for the same compositional section use the white mica solution model including Mg- and Fe-celadonite. In the pseudo-AFM (Fig. 5b), every assemblage contains white mica, quartz, and water. Phases like garnet or biotite occupy large single-phase stability fields. This diagram is not comparable to an ordinary AFM diagram. It still visualizes assemblages as a function of the bulk composition; however, the compositions of the phases are not related to their positions in the diagram. An equivalent diagram to Figure 5b was proposed by Miyashiro and Shido (1985), using a true AFM projection from a variable composition phengite.

The advantage of removing the pure muscovite constraint is that predicted assemblages become more realistic. For instance, a bulk composition for which we might expect stable biotite and K-feldspar, based on Figure 5a, is predicted to grow garnet and biotite. Furthermore, the single-phase field for garnet, as observed in the high-pressure assemblage of sample TN205 (Fig. 2a) is clearly not limited to a very narrow range of bulk compositions. For a general overview of phase relations in metapelites however, the classical AFM diagram still remains the most useful tool.

The combination of equilibrium assemblage diagrams with thermobarometry

A general observation from calculating many equilibrium phase diagrams in the last decade, is that the size and position of predicted stability fields is often not strongly dependent on various solution models, but mainly on the end-member properties of the phases. On the other hand, the predicted compositions are very dependent on the solution models. To predict the correct concentrations, the solution models must incorporate the complete compositional range of the minerals. At present, there is no reliable model for e.g., Ti in most silicates, Fe^{3+} in most minerals, Cl

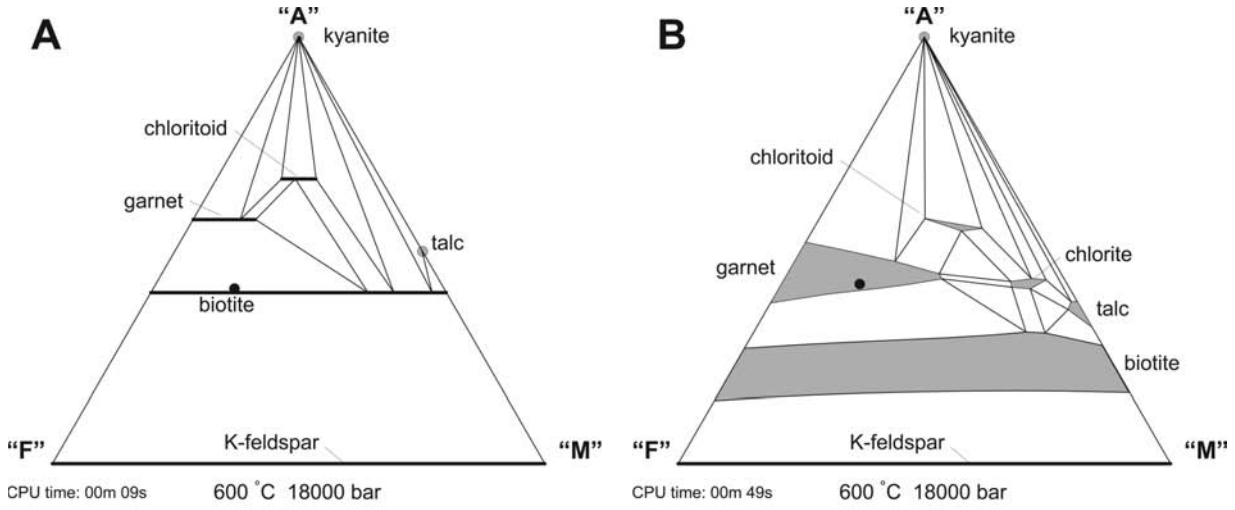

FIGURE 5. Pseudo-AFM diagrams. (**a**) Calculated with pure muscovite; (**b**) calculated with a white mica solution model containing celadonite. The black circle is the approximate composition of sample TN205. All assemblages contain additional white mica (or muscovite), quartz, and water. The single-phase fields are shaded; triangles are three-phase fields. The stretching of the single-phase fields (+Ms,Qtz,H_2O) in **b** is the result of the compositional variation of white mica.

and F in most hydrous phases, etc. Our predictions are therefore always restricted to simplified systems (but still yielding useful information). One case where the observed compositions could be adequately covered by the solution models is garnet-omphacite described by Meyre et al. (1997). In general, predicted compositions show correct trends but are seldom precise.

Here the more classic approach of thermobarometry has a distinct advantage. Instead of complete solution models including all end-member properties, only the activities of some end-members are required. The disadvantage of thermobarometry is that there is some uncertainty whether, and which compositions of all minerals used in the calculation equilibrated at the same time (and at the same *P* and *T*) and which other phases might have been present. Clearly, thermobarometry and equilibrium assemblage diagrams are complementary tools destined to be used together: Equilibrium assemblage diagrams provide a certain confidence on stable assemblages and supply important information constraining *P-T* paths, and thermobarometry furnishes reliable *P-T* estimates for specific points on a *P-T* path (e.g., near-peak conditions, prograde conditions from mineral inclusions).

This approach is demonstrated in Figure 6, using the TWQ software (Berman 1988, 1991; Berman and Aranovich 1996). TWQ uses a set of internally consistent thermodynamic data, i.e., thermodynamic properties of each mineral are consistent with phase equilibrium experiments and direct measurements of mineral properties (e.g., S, V, C_P). Thus, each mineral has the same thermodynamic properties in each reaction in which it participates. The database is the same JUN92, used mostly throughout this paper.

Sample 7744 (provided by R.G. Berman, personal communication) is a garnet-sillimanite-biotite-quartz-plagioclase-ilmenite metapelite collected from the Committee Bay belt of the north-central Canadian Shield. Subhedral, variably embayed garnet porphyroblasts up to 6 mm in diameter are enveloped by the foliation defined by biotite and sillimanite laths. Sparse cordierite forms irregular patches around some garnet rims, suggesting formation, together with some late biotite, via garnet breakdown.

Mineral compositions are given in Table 1. Garnet porphyroblasts display little compositional zoning, with Fe/(Fe+Mg) = 0.82–0.83, X_{Ca}^{Grt} = 0.031–0.035, and X_{Mn}^{Grt} decreasing slightly from core (X_{Mn}^{Grt} = 0.046) to rim (X_{Mn}^{Grt} = 0.032). Within ~0.4 mm of garnet rims adjacent to quartz or plagioclase, Fe/(Fe+Mg) increases to 0.86. Little compositional variation exists in matrix biotite [Fe/(Fe+Mg) = 0.53–0.54] or in plagioclase that forms matrix grains and rare inclusions in garnet (X_{An}^{Pl} = 0.22–0.26). *P-T* conditions of ~4.4 kbar—615 °C are recorded by garnet rims and adjacent biotite that is separated from garnet by plagioclase. Lack of biotite inclusions within garnet precludes calculation of earlier *P-T* conditions.

The whole-rock chemistry (in moles), determined from the offcut of the thin section used to measure mineral compositions, is SiO_2(69.47), Al_2O_3(11.32), CaO(1.89), MgO(5.23), FeO(7.61), K_2O(1.87), Na_2O(2.56) + excess H_2O. The calculated *P-T* from TWQ and the observed peak assemblage (Grt-Sil-Bt-Pl-Qz) with late Cd rimming Grt is in excellent agreement with the predicted equilibrium assemblage. A clockwise *P-T* path is implied by the observation of relic staurolite as inclusions in garnet, as well as cordierite forming rims around garnet.

In this example, the results from thermobarometry are strongly supported by the equilibrium calculations. If the predicted stability field of the observed assemblage is far away from the *P-T* estimate, one ought to consider the possibility that the selected compositions were not quenched at the same time.

Comparison of databases

Databases incorporate decades of experimental work and field experience and should be treated with respect. The ones we use were carefully compiled to be "internally consistent," i.e., the data are consistent with all experiments and observations. Differences between databases do exist however, because not all

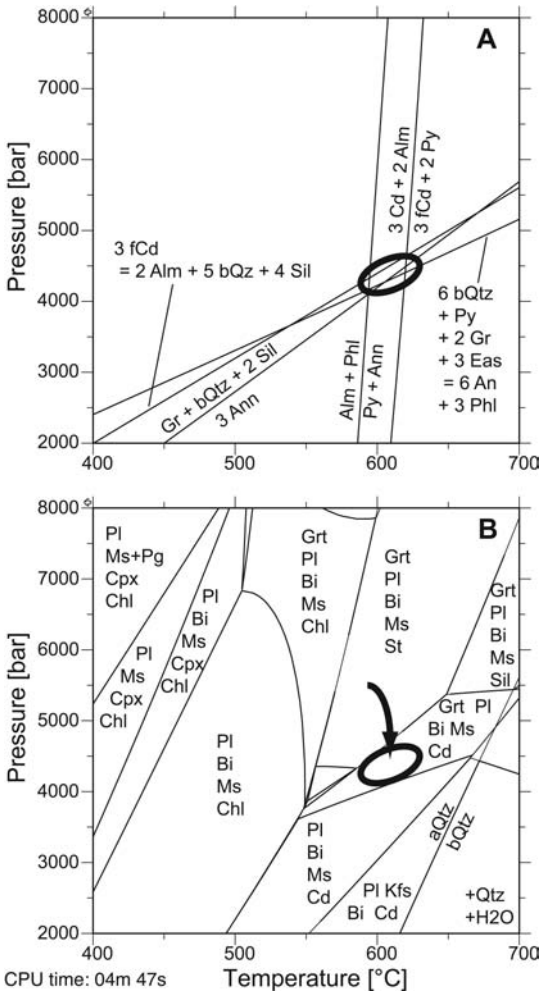

Figure 6. Combined information from thermobarometry and equilibrium assemblage diagrams. Sample 7744 (provided by R.G. Berman, personal communication) is a garnet-sillimanite-biotite-quartz-plagioclase-ilmenite metapelite collected from the Committee Bay belt of the north-central Canadian shield. (**a**) *P-T* estimation using mineral compositions and TWQ software yields ca. 615 °C, 4400 bar. (**b**) Equilibrium assemblage diagram for whole rock composition of sample 7744. Alm = almandine, An = Anorthite, Ann = Annite, Bi = biotite, Cd = cordierite, fCd = Fe-cordierite, Chl = chlorite, Cpx = clinopyroxene, Eas = eastonite, Gr = grossular, Grt = garnet, Kfs = K-feldspar, Ms = muscovite, Pg = paragonite, Phl = phlogopite, Pl = plagioclase, Py = pyrope, Qtz = quartz, Sil = sillimanite, St = staurolite.

Table 1. Composition of sample 7744 (wt%), a garnet-sillimanite-biotite-quartz-plagioclase-ilmenite metapelite collected from the Committee Bay belt of the north-central Canadian shield (R.G. Berman, personal communication)

	Mineral sample				
	Garnet rim	Feldspar	Cordierite	Biotite	Mica
	11	177	131	137	130
SiO_2	37.1	61.5	47.2	34.5	45.9
TiO_2	0.0	–	0.0	1.7	0.4
Al_2O_3	20.9	24.0	31.7	18.8	34.9
FeO	36.7	0.4	7.9	19.4	1.0
MgO	3.5	–	8.4	9.9	0.6
CaO	1.1	5.0	0.0	0.0	0.1
MnO	1.4	–	0.1	0.1	0.0
Na_2O	–	8.5	0.3	0.3	0.9
K_2O	–	0.1	0.7	8.9	9.8
Cr_2O_3	0.1	–	0.1	0.1	0.0
BaO	–	0.0	0.0	0.1	0.3
SrO	–	0.1	–	–	–
NiO	–	–	0.0	0.0	0.0
ZnO	–	–	0.0	0.1	0.0
V_2O_3	–	–	0.0	0.0	0.1
P_2O_5	–	–	–0.1	–0.5	0.0
F	–	–	0.1	1.1	0.0
Cl	–	–	0.0	0.0	0.0
Total	100.7	99.5	95.9	94.7	94.1

experiments are unambiguous and for some phases thermodynamic properties are only vaguely constrained. Therefore, data may differ by relatively large amounts, but still be internally consistent. Comparison of databases is not very common, because many programs are firmly tied to one specific database. TWQ, for instance, uses JUN92 (or the newer DEC06) and THERMOCALC 3.25 is linked to tcdb55. Theriak/Domino is not attached to a specific database. The only requirement is reformatting existing databases so they can be used as input. This task is not always straightforward. For instance, not all solution models used by THERMOCALC can be translated directly into a minimizable function. This concerns some models forcing an equipartitioning of Fe and Mg on several sites, which is described as "a logical inconsistency" by Holland and Powell (2006). For such solutions ΔG as calculated by THERMOCALC for a specific mineral composition is not at the minimum of the solution function as used in Theriak. Clearly, a minimization will never reproduce the distribution of species used to calibrate the model. To use these solutions for calculating equilibrium assemblage diagrams, equipartitioning is ignored. As discussed above, using a slightly different solution model does not significantly change the equilibrium assemblage diagrams. The predicted compositions will however not be consistent. In the examples shown in Figure 7, the only phase where this simplification may produce visible deviations is chlorite.

The diagrams in Figure 7 are for the same sample, TN205, as used for Figure 2. Figure 7a is calculated using the database JUN92 (Berman et al. 1988, with modifications), Figure 7b with tcdb55 (THERMOCALC v. 3.25). At first glance, the diagrams look quite different. Closer inspection however shows that corresponding stability fields are mostly within 20–40 °C and 1 kbar. Notably, the dehydration reactions of Pg and Ms are almost at identical positions. The staurolite stability field is predicted to be smaller in Figure 7b and differences at higher pressures also exist because tcdb55 includes a glaucophane solution model, not defined in JUN92. The largest discrepancies occur for assemblages including phases with most uncertain thermodynamic properties in both databases. Despite all these uncertainties however, we will reach the same conclusions for the petrogenesis of sample TN205 with either diagram.

Discussion

The strategy of Domino allows computing an almost unlimited diversity of equilibrium assemblage diagrams. The main reason for this flexibility is that the term "assemblage" is not restricted to a petrologic meaning but may be defined in many, even unconventional ways. Calculating single points, which

are later combined into lines, leads to robustness against occasional failures in the equilibrium calculations. For one diagram, typically 5000 to 10 000 equilibria are calculated. If for some reason, one or the other fails, this does not seriously affect the Domino algorithm.

We have addressed in the present paper many different types of diagrams that can be calculated with the Theriak/Domino software, but one should also be aware of some of its limitations. For instance, we cannot construct a classical petrogenetic grid, because a *P-T* equilibrium assemblage diagram is always restricted to a single bulk-chemical composition. To calculate a simple univariant reaction, an extensive modification of the database is required, removing all phases not participating and possibly adding solutions of fixed compositions. Diagrams that require a fixed phase composition like *T*-X(CO_2) diagrams can only be approximated by using, e.g., a ratio of solid to fluid of around 1:1 000 000. This forces the fluid composition to turn out at practically the desired value. Finally, diagrams showing isopleths and modal amounts could also be constructed using a more efficient computational approach than the brute force method of Domino, once the phase boundaries are known [e.g., the strategy used in the Gibbs program by Spear et al. (2001)].

The general philosophy of the Theriak/Domino software is that diagram construction is fully automatic, fast, and easy to use. All phases in a given database are considered and the stable assemblages are calculated by Gibbs free energy minimization. The only control a user has on the results is to modify the database and to vary the bulk system composition. The convenience and speed of diagram production emphasizes the value of the software not only for research, but also for learning and teaching.

It is expected that predicted equilibrium assemblage diagrams reflect at least the main features of observation. For example, calculated equilibrium assemblages and phase compositions should more or less agree with observed assemblages and mineral compositions. Inconsistencies help localize errors in the input constraints of the problem being considered. Such constraints generally include: (1) the validity of the database (standard thermodynamic data and solution models); (2) the assumption of equilibrium attainment at some scale of observation; and (3) the role of effective bulk composition at some stage of rock evolution.

It is worthy to stress the distinction between the bulk-rock composition, as typically expressed by chemical whole-rock analysis, and the effective bulk composition at some evolutionary stage of a rock that might result, for example, from element fractionation into some "refractory" phases. Similarly obvious is the significance of the scale of assumed local equilibrium on which the interpretation of a calculated equilibrium assemblage diagram relies. Post-peak processes, especially in high-grade rocks (e.g., by inter-granular diffusion), may significantly modify the equilibrium phase compositions in a manner that is not accompanied and/or detectable in the mineralogical composition of the rock. Up-to-date experience with the application of computer-based calculation of equilibrium assemblage diagrams shows that the major source of problems and difficulties a typical user has to address roots in the effective bulk and equilibrium assumption. Dealing with problems associated with the validity of the database requires a profound knowledge of experimental techniques and their uncertainties.

At the present time, it is not possible to reproduce natural processes, including all minor elements and accessories by thermodynamic modeling. The calculation of equilibrium assemblage diagrams should be considered above all as a thought-provoking exercise, toward a better understanding of nature. Often the most unexpected or, according to our own prejudice, even wrong results lead to the deepest insights.

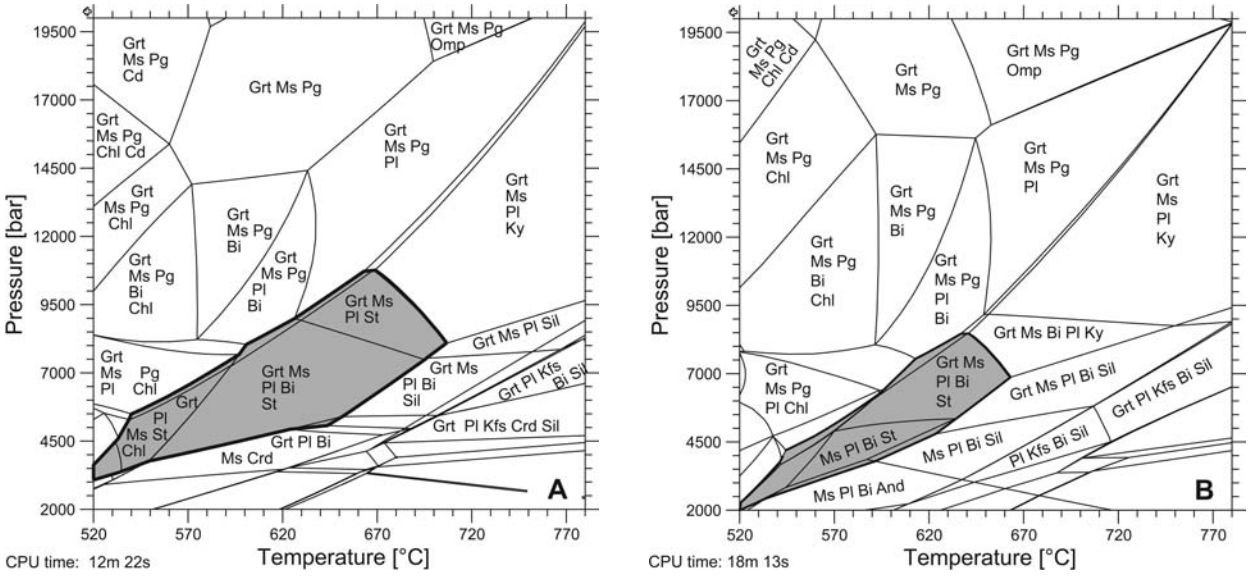

FIGURE 7. Comparison of databases. Sample TN205 (see also Fig. 2). The staurolite field is shaded, not all assemblages are labeled. Bi = biotite, Chl = chlorite, Grt = garnet, Kfs = K-feldspar, Ky = kyanite, Ms = muscovite, Pg = paragonite, Pl = plagioclase, Sil = sillimanite, St = staurolite, Omp = omphacite. (**a**) Equilibrium assemblage diagram calculated with the database JUN92. (**b**) With database tcdb55.

ACKNOWLEDGMENTS

The authors thank R.G. Berman for the elaboration of sample 7744, F. Gaidies for comments on an earlier version, and F. Spear and an anonymous reviewer who substantially helped to make the manuscript comprehensible. The development of the Domino software was in some cases actively, but in most cases unintentionally assisted by T. Brown, H. Greenwood, R. Berman, M. Engi, T. Parra, L. Aranovich, K. Bucher, R. Bousquet, M. Kirschen, C. Meyre, T. Nagel, P. Hunziker, F. Gaidies, and D. Pattison.

REFERENCES CITED

Becke, F. (1904) Über Mineralbestand und Struktur der kristallinischen Schiefer. Congrès géologique internnational, Compte rendu de la IX. session, Vienne 1903.

Berman, R.G. (1988) Internally-consistent thermodynamic data for minerals in the system Na_2O-K_2O-CaO-MgO-FeO-Fe_2O_3-Al_2O_3-SiO_2-TiO_2-H_2O-CO_2. Journal of Petrology, 29, 445–522.

——— (1991) Thermobarometry using multiequilibrium calculations: A new technique, with petrological applications. Canadian Mineralogist, 29, 833–856.

Berman, R.G. and Aranovich L.Y. (1996) Optimized standard state and solution properties of minerals. I. Model calibration for olivine, orthopyroxene, cordierite, garnet and ilmenite in the system FeO-MgO-CaO-Al_2O_3-TiO_2-SiO_2. Contributions to Mineralogy and Petrology, 126, 1–24.

Bousquet, R., Goffé, B., de Capitani, C., Chopin, C., Le Pichon, X., and Henry, P. (2005) Comment on "Subduction factory 1. Theoretical mineralogy, densities, seismic wave speeds and H_2O contents" by Hacker, B., Abers, G.A., and Peacock, S.M. Journal of Geophysical Research, 110, B02206.

Coggon, R. and Holland, T.J.B (2002) Mixing properties of phengitic micas and revised garnet-phengite thermobarometers. Journal of Metamorphic Geology, 20, 683–696.

Connolly, J.A.D. (1990) Multi-variable phase diagrams: An algorithm based on generalized thermodynamics. American Journal of Science, 290, 666–718.

de Capitani, C. (1994) Gleichgewichts-Phasendiagramme: Theorie und Software. Berichte der Deutschen Mineralogischen Gesellschaft, 6, 48.

de Capitani, C. and Brown, T.H. (1987) The computation of chemical equilibrium in complex systems containing non-ideal solutions. Geochimica et Cosmochimica Acta, 51, 2639–2652.

Eskola, P. (1915) On the relations between the chemical and mineralogical composition in the metamorphic rocks of the Orijarvi region. Bulletin de la Commission géologique de Finlande, 44, 1–107 (in Finnish), 109–145 (in English).

——— (1922) The mineral facies of rocks. Norsk Geologisk Tidsskrift (Norwegian Journal of Geology), 6, 143.

Gaidies, F., de Capitani, C., and Abart, R. (2008a) THERIA_G: a software program to numerically model prograde garnet growth. Contributions to Mineralogy and Petrology, 155, 657–671.

Gaidies, F., de Capitani, C., Abart, R., and Schuster, R. (2008b) Prograde garnet growth along complex *P-T-t* paths: Results from numerical experiments on polyphase garnet from the Wölz Complex (Austroalpine basement). Contributions to Mineralogy and Petrology, 155, 673–688.

Goldschmidt, V.M. (1912a) Geologisch-petrographische Studien im Hochgebirge des südlichen. Norwegens. I. Ein kambrisches Konglomerat von Finse und dessen Metamorphose. Skrifter utgit av Videnskapsselskapet i Kristiania. I. Matematisk-naturvidenskabelig klasse, 18.

——— (1912b) Geologisch-petrographische Studien im Hochgebirge des südlichen. Norwegens. II. Die kaledonische Deformation der südnorwegischen Urgebirgstafel. Skrifter utgit av Videnskapsselskapet i Kristiania. I. Matematisk-naturvidenskabelig klasse, 19.

Grubenmann, U. and Niggli, P. (1924) Die Gesteinsmetamorphose, vol. 1, 539 p. Borntraeger, Berlin.

Holland, T.J.B. and Powell, R. (2006) Mineral activity-composition relations and petrological calculations involving cation equipartition in multisite minerals: A logical inconsistency. Journal of Metamorphic Geology, 24, 851–861.

Hunziker, P. (2003) The stability of tri-octahedral Fe^{2+}-Mg-Al chlorite. A combined experimental and theoretical study. Ph.D. thesis, University of Basel, Switzerland.

Keller, L.M., de Capitani, C., and Abart, R. (2005) A quaternary solution model for white micas based on natural coexisting phengite-paragonite pairs. Journal of Petrology, 46, 2129–2144.

Massonne, H.-J. and Schreyer, W. (1987) Phengite geobarometry based on the limiting assemblage with K-feldspar, phlogopite and quartz. Contributions to Mineralogy and Petrology, 96, 212–224.

Meyre, C., de Capitani, C., and Partzsch, J.H. (1997) A ternary solid solution model for omphacite and its application to geothermobarometry of eclogites from the Middle Adula nappe (Central Alps, Switzerland). Journal of Metamorphic Geology, 15, 687–700.

Miyashiro, A. and Shido, F. (1985) Tschermak substitution in low- and middle-grade pelitic schists. Journal of Petrology, 26, 449–487.

Nagel, T., de Capitani, C., and Frey, M. (2002) Isograds and *P-T* evolution in the eastern Lepontine Alps (Graubünden, Switzerland). Journal of Metamorphic Geology, 20, 309–324.

Pattison, D.R.M. and Tinkham, D.K. (2009) Interplay between equilibrium and kinetics in prograde metamorphism of pelites: An example from the Nelson aureole, British Columbia. Journal of Metamorphic Geology, 27, 249–279.

Powell, R. and Holland, T.J.B. (1994) Optimal geothermometry and geobarometry. American Mineralogist, 79, 120–133.

Powell, R., Holland, T.J.B., and Worley, B. (1998) Calculating phase diagrams involving solid solutions via nonlinear equations, with examples using THERMOCALC. Journal of Metamorphic Geology, 16, 577–588.

Spear, F.S. (2004) Fast cooling and exhumation of the Valhalla Metamorphic Core Complex, Southeastern British Columbia. International Geology Review, 46, 193–209.

Spear, F.S. and Markussen, J.C. (1997) Mineral zoning, P-T-X-M phase relations and metamorphic evolution of some Adirondack granulites, New York. Journal of Petrology, 38, 757–783.

Spear, F.S., Kohn, M.J., and Cheney, J.T. (1999) *P-T* paths from anatectic pelites. Contributions to Mineralogy and Petrology, 134, 17–32.

Spear, F.S., Pyle, J.M., and Storm, L.C. (2001) Short course: Thermodynamic modeling of mineral reactions: An introduction to Program Gibbs. Northeast Section, Geological Society of America, Burlington, Vermont.

Thompson, J.B. (1957) The graphical analysis of the mineral assemblages in pelitic schists. American Mineralogist, 42, 842–858.

Tinkham, D.K., Zuluaga, C.A., and Stowell, H.H. (2001) Metapelite phase equilibria modeling in MnNCKFMASH: The effect of variable Al_2O_3 and MgO/(MgO+FeO) on mineral stability. Geological Materials Research, 3, 1–42.

MANUSCRIPT RECEIVED JULY 24, 2009
MANUSCRIPT ACCEPTED FEBRUARY 9, 2010
MANUSCRIPT HANDLED BY EDWARD GHENT